




Key Role of Cytochrome C for Apoptosis Detection Using Raman Microimaging in an Animal Model of Brain Ischemia with Insulin Treatment.

Item Type	Article
Authors	Russo, Vanessa; Candeloro, Patrizio; Malara, Natalia; Perozziello, Gerardo; Iannone, Michelangelo; Scicchitano, Miriam; Mollace, Rocco; Musolino, Vincenzo; Gliozzi, Micaela; Carresi, Cristina; Morittu, Valeria M; Gratterer, Santo; Palma, Ernesto; Muscoli, Carolina; Di Fabrizio, Enzo M.; Mollace, Vincenzo
Citation	Russo, V., Candeloro, P., Malara, N., Perozziello, G., Iannone, M., Scicchitano, M., ... Mollace, V. (2019). Key Role of Cytochrome C for Apoptosis Detection Using Raman Microimaging in an Animal Model of Brain Ischemia with Insulin Treatment. Applied Spectroscopy, 000370281985867. doi:10.1177/0003702819858671
Eprint version	Post-print
DOI	10.1177/0003702819858671
Publisher	SAGE Publications
Journal	Applied spectroscopy
Rights	Archived with thanks to Applied spectroscopy
Download date	04/08/2022 16:32:49
Link to Item	http://hdl.handle.net/10754/656412

Key Role of Cytochrome C for Apoptosis Detection Using Raman Microimaging in an Animal Model of Brain Ischemia with Insulin Treatment

Vanessa Russo^{1,2,*}, Patrizio Candeloro^{3,*} , Natalia Malara^{1,3}, Gerardo Perozziello³, Michelangelo Iannone⁴, Miriam Scicchitano¹, Rocco Mollace¹, Vincenzo Musolino^{1,5}, Micaela Gliozzi^{1,5}, Cristina Carresi^{1,5}, Valeria M. Morittu¹, Santo Gratterer¹, Ernesto Palma^{1,5}, Carolina Muscoli^{1,5,6}, Enzo Di Fabrizio^{3,7}, and Vincenzo Mollace^{1,5,6}

Applied Spectroscopy

0(0) 1–10

© The Author(s) 2019

Article reuse guidelines:

sagepub.com/journals-permissions

DOI: 10.1177/0003702819858671

journals.sagepub.com/home/asp



Abstract

Brain ischemia represents a leading cause of death and disability in industrialized countries. To date, therapeutic intervention is largely unsatisfactory and novel strategies are required for getting better protection of neurons injured by cerebral blood flow restriction. Recent evidence suggests that brain insulin leads to protection of neuronal population undergoing apoptotic cell death via modulation of oxidative stress and mitochondrial cytochrome c (CytC), an effect to be better clarified. In this work, we investigate on the effect of insulin given intracerebroventricular (ICV) before inducing a transient global ischemia by bilateral occlusion of the common carotid arteries (BCCO) in Mongolian gerbils (MG). The transient (3 min) global ischemia in MG is observed to produce neurodegenerative effect mainly into CA3 hippocampal region, 72 h after cerebral blood restriction. Intracerebroventricular microinfusion of insulin significantly prevents the apoptosis of CA3 hippocampal neurons. Histological observation, after hematoxylin and eosin staining, puts in evidence the neuroprotective role of insulin, but Raman microimaging provides a clearer insight in the CytC mechanism underlying the apoptotic process. Above all, CytC has been revealed to be an outstanding, innate Raman marker for monitoring the cells status, thanks to its resonant scattering at 530 nm of incident wavelength and to its crucial role in the early stages of cells apoptosis. These data support the hypothesis of an insulin-dependent neuroprotection and antiapoptotic mechanism occurring in the brain of MG undergoing transient brain ischemia. The observed effects occurred without any peripheral change on serum glucose levels, suggesting an alternative mechanism of insulin-induced neuroprotection.

Keywords

Raman microspectroscopy, brain ischemia, Raman spectra multivariate analysis, insulin neuroprotection, cytochrome c, CytC

Date received: 10 February 2019; accepted: 30 May 2019

Introduction

Brain ischemia is one of the leading causes of death and disability worldwide.¹ Neurodegenerative disorders which

follow ischemic stroke occur as a result of a series of pathophysiological events including glutamate-mediated

¹IRC-FSH Interregional Center for Food Safety and Health, University “Magna Graecia” of Catanzaro, Italy

²Association: Exchanger-Share Your Science, Complesso “Nini Barbieri,” Catanzaro, Italy

³BioNEM Laboratory, Department of Clinical and Experimental Medicine, University “Magna Graecia” of Catanzaro, Italy

⁴CNR, Neuroscience Institute, Pharmacology Section, Complesso “Nini Barbieri,” Catanzaro, Italy

⁵Nutramed S.C.A.R.L., Complesso “Nini Barbieri”, Roccelletta di Borgia, Catanzaro, Italy 88100

⁶Centro del farmaco (IRCCS), Rome, Italy

⁷KAUST (King Abdullah University of Science and Technology), PSE and BESE Divisions, Thuwal, Kingdom of Saudi Arabia

*Equal contributors.

Corresponding author:

Patrizio Candeloro, Università degli Studi “Magna Graecia” di Catanzaro, Campus Universitario - Loc. Germaneto, Catanzaro, 88100 Italy.

Email: patrizio.candeloro@unicz.it

excitotoxicity, calcium overload, inflammation, oxidative stress, stress signaling, and both apoptotic and necrotic neuronal cell death.^{1,2} Although many studies have proven the protective effects of natural as well as synthetic compounds in patients undergoing ischemic stroke,^{3–6} the limited time window during which these compounds have clinical utility and their adverse side effects restrict their application in practice. Thus, therapeutic intervention for getting better neuroprotection of post-ischemic brain tissue is still unsatisfactory and the majority of patients post-stroke display a poor prognosis such as long-term physical disability and memory disturbances.⁷ Therefore, it is still important to explore new therapeutic targets and post-stroke strategies including interventions in the supply of oxygen and substrates as well as their better utilization in order to attenuate consequences of cerebral blood flow restriction.

It is well known that hyperglycemia and/or diabetes potentially exacerbate the neuronal damage observed after ischemic stroke (for a review, see Shinichi et al.⁸) and that hyperglycemia/glucose intolerance may be induced by cerebral ischemic stress. The normalization of blood glucose levels during the first 48 h of hospitalization appears to confer greater survival outcomes in stroke patients. On the other hand, poor glycemic control appears to be associated with large infarct size, poor clinical outcomes, and a higher risk of mortality after ischemic stroke.⁸ Besides this evidence, the mechanism underlying post-ischemic imbalanced glucose modulation and the role of endogenous factors regulating glucose utilization in post-ischemic brain tissues, including insulin receptors (IRs), remains still unclear. Evidence exists that insulin can cross the blood–brain barrier (BBB) and that specific IRs are located on both macrovascular and microvascular brain circulation.⁹ Recent data also show that IRs are widespread, distributed in the central nervous system (CNS) being located in the olfactory bulb, cerebral cortex, hippocampus, hypothalamus, cerebellum, and that choroid plexus have the highest IR density^{10–12} even if the hypothalamus, the hippocampus, and the cerebellum have higher densities.¹³ It is worth saying that the neuroprotective role of insulin could help the patients after the ischemic event, in the first 24–48 h of hospitalization, and that it is not proposed for stroke prevention.

In this work, the neuroprotective role of insulin, administered to Mongolian gerbils (MG; *Meriones unguiculatus*) before a transient global ischemia, is used as animal model for emphasizing the key role of cytochrome c (CytC) in apoptosis detection by Raman imaging. Standard histological observation, after suitable staining, highlights the beneficial effects of insulin, above all in the CA3 hippocampal region. However, Raman microimaging offers the possibility to better understand the biochemical mechanisms with relatively small expenditures in terms of time and labor. It is worth mentioning that Raman microspectroscopy has

attracted a large interest from the biochemistry/biomedical community in the last decade and several works have been proposed regarding lipidomics,^{14,15} proteomics,^{16,17} stem cells differentiation,¹⁸ cancer stem cell biochemistry,¹⁹ investigation of exosomes derived from tumor cells,²⁰ comparative studies of embryonic stem cells, and induced pluripotent stem cells.^{21,22} In addition, in the field of brain tissue analysis, several works have been using Raman spectroscopy with different purposes, such as the determination of brain edema in tumor diseases,²³ imaging of brain injury where Raman signatures are correlated to apoptosis by evidencing a Caspase over-expression through immunohistochemistry,²⁴ label-free tissue imaging,²⁵ investigation of the neuroprotective role of ascorbic acid against brain injury due to oxidative stress,²⁶ and, very recently, Raman spectroscopy in combination with PCA analysis has been used to discriminate between normal, ischemic, and nNOS inhibitor-treated brain tissues after ischemic events.²⁷ It is worth saying that this last work is a very preliminary one, since no tissue imaging has been performed and a very limited number of spectra (10 spectra) has been collected for each kind of tissue.

Typical advantages of Raman microspectroscopy are nearly no preparation of the sample before measurements and label-free approach, thus meaning that no dyes or other labels are required. In addition, since the Raman effect relies on light scattering from molecular vibrations, it can potentially detect several classes of biomolecules simultaneously (from proteins and lipids to DNA/RNA, to saccharides and other metabolites), and this constitutes its most valuable feature for biochemical analysis of cells and tissues, especially when different molecules need to be followed or it is still unknown the molecular interplay in a biological pathway. On the other hand, this richness of provided data on several biomolecules classes at once will require more sophisticated tools for data analysis, such as multivariate approaches.

Material and Methods

Surgical Procedures, Insulin Administration, Bilateral Common Carotid Artery Occlusion

Adult male MGs (body weight, 50–70 g; Charles River, Milan, Italy) were housed in a conventional state under adequate temperature (20 °C) and humidity (60%) with a 12/12 h light/dark cycle and were provided with free access to water and food. "Principles of Laboratory Animal Care" were followed and gerbils were treated and sacrificed in accordance with approved Italian Ministerial procedures appropriate to the species. Experiments were approved by the local ethics commission.

Under Zoletil/Domitor (30 mg/kg, intraperitoneal) anesthesia, a cannula was positioned using a stereotaxic apparatus; 1 μ L (0.1 IU/Kg) of insulin was slowly infused 5 min before the induction of ischemia into the third ventricle

according to the coordinates of Paxinos and Watson's atlas (AP = -1.3 mm, L = 0 mm, H = 4.5).

Brain ischemia was induced by temporary bilateral occlusion of the common carotid artery (BCCO). Under Zoletil/Domitor (30 mg/kg, i.p.) anesthesia, the common carotid arteries were dissected via a ventral neck incision and occluded with ligatures for 3 min (day 0). The ligatures were then removed, the skin incision sutured, and the animals allowed to recover. Postoperative recovery was confirmed by careful animal observation and Doppler analysis confirmed cerebral blood flow restoring. Reperfusion was followed for three days after surgical procedures.

Sham-operated animals, serving as controls, were subjected to the same surgical procedures except that the common carotid arteries were not occluded.

Hence, we have three groups of animals, named "BCCO", "Ins.+BCCO", and "Sham" in the following: (1) MG subjected to 3 min of ischemia by BCCO followed by 72 h of reperfusion (BCCO group); (2) MG treated with insulin 5 min before inducing BCCO and undergoing 72 h of reperfusion (Ins.+BCCO group); and (3) MG subjected to surgical procedure alone without causing ischemia (Sham group).

Neuropathological Studies

Three days after BCCO, the gerbils were re-anesthetized with Zoletil/Domitor (100 mg/kg, i.p.) and transcardially perfusion-fixed with phosphate buffered solution and subsequently with 4% buffered formaldehyde (pH 7.4) after a brief rinse with saline and heparin (0.1%) at room temperature. The brains were explanted and fixed in 4% paraformaldehyde solution (Bioptica) for one week at room temperature, dehydrated by gradual transitions in ethanol, and embedded in paraffin (Bioplast, biopsy). Briefly, coronal slices of the dorsal hippocampus 7 μm thick were cut with a vibratome for hematoxylin and eosin staining (H&E, Bioptica). The sections were cover slipped with permount and examined using a light microscope (Olympus BX53).

Raman Microimaging

For Raman studies, the brains explanted from sacrificed animals were rapidly frozen in optimal cutting temperature (OCT) blocks in liquid nitrogen and then stored at -80°C . Coronal slices of the dorsal hippocampus 50 μm thick were cut with a cryostat, dried for 1 h, and analyzed using Raman microspectroscopy. In this way, chemicals for fixation and/or staining are avoided, preventing their potential influences on Raman spectra.

Raman mapping measurements were performed with an Alpha 300R microscope from WITec GmbH, equipped with a 532 nm laser source and in backscattering configuration. The total laser power at the sample level is set to 10 mW to avoid tissue photodamage and the light is focused on the

sample through a $20\times/0.4$ NA objective. A 600 lines/mm grating is used for frequency analysis of the backscattered light, with a spectral resolution of about 3 cm^{-1} . For each brain tissue, an area of $120 \times 80\ \mu\text{m}$ in the CA3 hippocampal region was mapped through a raster scan, with a step size of $2\ \mu\text{m}$. For each pixel, spectra are recorded in the spectral range of $400\text{--}3100\text{ cm}^{-1}$, with an accumulation time of 3 s. Before each Raman session, the Raman shift has been calibrated measuring spectra on a Silicon sample and using as a reference the sharp peak at 520 cm^{-1} , typical of Si. The 50 μm thickness of the brain tissues was enough to prevent Raman signal coming from the bottom glass slide.

Raman Spectra Analysis

After Raman measurements, some preprocessing steps were carried out on the spectra before multivariate analysis. They were first normalized to the total spectral area²⁸ and then divided in two spectral regions: the $400\text{--}1800\text{ cm}^{-1}$ region, the so-called fingerprint region; and the $2600\text{--}3100\text{ cm}^{-1}$ region, where CH_2 and CH_3 stretching vibrations are located. Subsequently, the fingerprint region undergoes a fourth order polynomial subtraction accounting for fluorescence effects, while in the latter region a simply first order line was enough for correcting the slope of the spectra. Finally, principal component analysis (PCA) and K-means cluster analysis (KCA) were performed separately in the two spectral regions. In order to compare the results of these multivariate techniques between the different groups of animals, the recorded spectra were processed altogether as one single group at once. By doing so, the computed principal components (PC) are the same through all the animal groups. Starting from both PCA and KCA, pseudocolor maps were produced for a fast visualization of multivariate results. In the former, the scores of PCA were mapped as a function of the x,y spatial coordinates, where brighter colors correspond to higher score values and darker colors to lower score values. Instead, in the latter (KCA), one color was assigned to each cluster and the spatial distribution of each cluster was mapped in the x,y space. General overviews of multivariate approaches applied to Raman spectroscopy can be found in Matthaus et al.²⁹ and Rajalahti et al.³⁰ All the preprocessing and multivariate analysis were performed with the Raman Tool Set software package that is freely available (<http://ramantoolset.sourceforge.net>).³¹

Results and Discussion

Effects of Insulin on Apoptotic Cell Death of Hippocampal Neurons: Histological Analysis

Three days after inducing global cerebral ischemia via BCCO, damage was detected in the hippocampus and in large areas of the neocortex (Fig. 1).

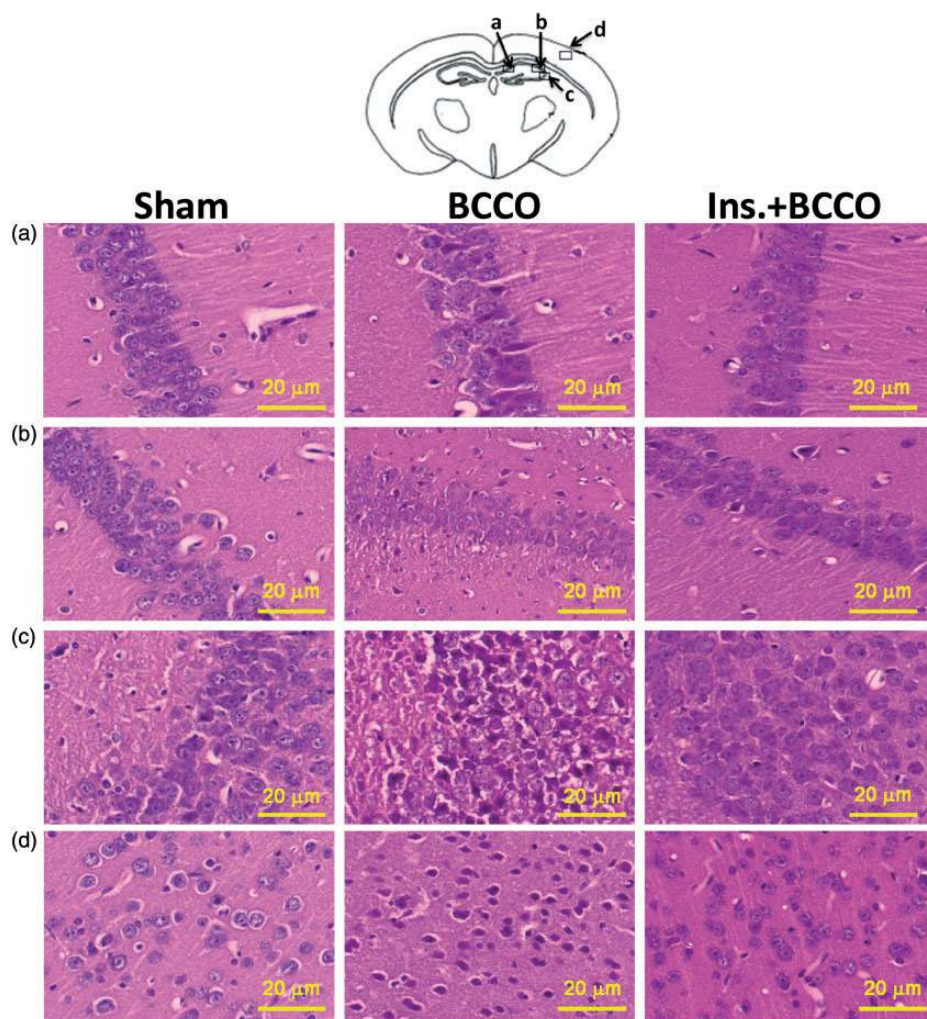


Figure 1. Insulin protects against neuronal cell death in the CA1, CA2, CA3 hippocampus and neocortex. Representative photomicrographs of gerbil brain sections stained with H&E. Pathologic features of brain sections at 72 h after global brain ischemia by bilateral occlusion of the common carotid for 3 min are observable in the middle column (BCCO). (a) CA1 region of pyramidal cell layer; (b) CA2 region of pyramidal cell layer; (c) CA3 region of pyramidal cell layer; and (d) somatic sensory area of the cerebral cortex. It is clear that the presence of pyknotic nuclei and neuronal degeneration in the area CA3 (c) hippocampus, in particular, of the animal subjected to cerebral ischemia by BCCO compared to sham control and treated with insulin before ischemia (Ins.+ BCCO). Cell changes are also evident in the parietal cortex somato-sensory area (d) of ischemic gerbil (BCCO). Scale bar = 20 µm, cellSens Dimension software.

In particular, in gerbils with from ischemia/reperfusion (BCCO group), marked signs of cellular degeneration of neurons in CA1–CA2 and CA3 hippocampus areas were observed, compared to tissues of sham-operated animals (CA1, CA2, and CA3 are standard names used in anatomy for three different areas of the hippocampus, the CA acronym coming from the Latin *Cornu Ammonis*). In addition, histological analysis showed a marked gliosis, condensation of the cytoplasm, and the presence of numerous cells with pyknotic nuclei (pyknosis is a degenerative process of the cellular nucleus, occurring under conditions of cell death due to apoptosis or necrosis). Moreover, various areas exhibit the so-called “coarctation of the cell” (a cell size narrowing). Widespread signs of neurodegeneration were

also evident in the load of the parietal cortex, particularly in the somatosensory area.

Conversely, the presence of significant neurodegenerative events in the animals treated with insulin (0.1 IU/kg) was not detected (Ins.+BCCO group).

Cytochrome C Release and Lipid Peroxidation: Raman Microimaging

Raman Spectroscopy of Brain Tissue. Raman microspectroscopy was performed on the CA3 hippocampal area, which proved to be particularly vulnerable to ischemic insult. As a first point, it should be noted that the absorption spectrum of CytC exhibits a small peak centered at

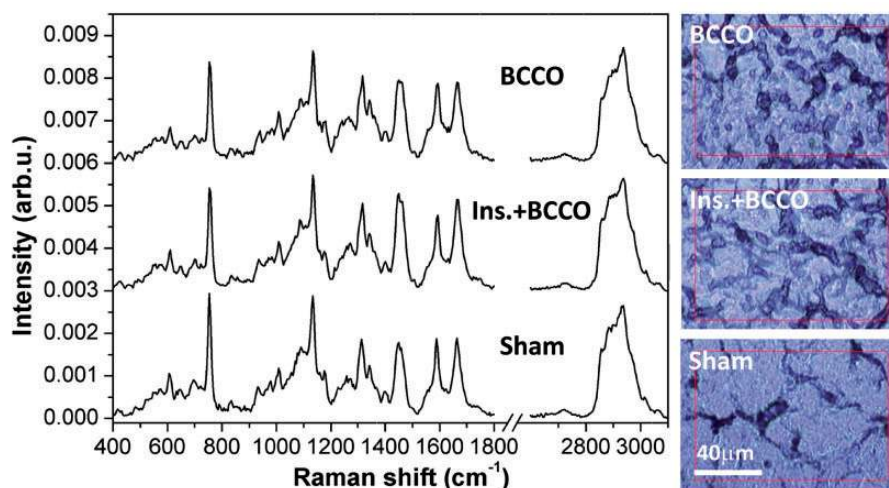


Figure 2. Raman average spectra. Raman microimaging has been used for recording vibrational spectra maps of the brain tissues of Sham, Ins.+BCCO, and BCCO animals. On the left, for each animal group, the average spectra are shown in the two different spectral regions: the so-called fingerprint region at 400–1800 cm^{-1} and the 2600–3100 cm^{-1} region typical of CH_2 and CH_3 stretching vibrations. On the right, optical microscope pictures of the three brain tissues are reported: the mapped area, evidenced by the rectangular line, is $120 \times 80 \mu\text{m}$ and Raman spectra are collected with a stepsize of 2 μm .

530 nm,³² so that resonant Raman scattering of CytC is expected to occur using a 532 nm laser source. This means that CytC peaks will be enhanced compared to other biomolecules. We performed Raman mapping of the CA3 hippocampal area of Sham, BCCO, and Ins.+BCCO animal groups.

Figure 2 shows the spectra averaged over the whole mapped area for the Sham, BCCO, and Ins.+BCCO animals. At a first glance, it can be noted that the spectra are very similar to each other and no evident differences are exhibited. All of the three spectra show the typical Raman features of both cells and tissues signals. Starting from the higher frequencies, we can observe the Raman peak of CH_3 stretching vibrations at 2950 cm^{-1} , occurring more in proteins than in lipids, and the CH_2 vibrations at 2850 cm^{-1} , conversely more in lipids than in proteins.³³ In the fingerprint region, we find the amide I vibration at about 1660 cm^{-1} , partly overlapped by the $\text{C}=\text{C}$ stretching, and the CH_2 deformation at 1445 cm^{-1} ; in the 1250–400 cm^{-1} region, there is an overlapping of Amide III, nucleic acids, and fatty acid signals. Finally, the sharp peak of phenylalanine is clearly visible at 1005 cm^{-1} . Besides these characteristic features common to most Raman spectra from cells and tissues, we have four strong peaks located at approximately 1584, 1315, 1127, and 750 cm^{-1} , corresponding to different CytC vibrations as already discussed in literature (for a recent CytC Raman spectrum, see Read et al.,³⁴ while for peak assignment, see Hu et al.³⁵).

Principal Component Analysis and K-Means Cluster Analysis of Raman Maps. Principal component analysis was performed on the whole data set of spectra collected on the three samples. This means that all the spectra coming from Sham,

BCCO, and Ins.+BCCO animals have been put together to produce a larger ensemble over which the PCA was performed. This ensures that the computed PCs are exactly the same through the whole spectral data set. As is well known, in PCA analysis, the first PCs are the most significant ones since they retain the largest part of spectral information. In the following analysis, PC1 in the 2600–3100 cm^{-1} range (holding 39% of data variance) and PC3 in the 400–1800 cm^{-1} range (holding 15% of variance) provide significant information on the biochemistry of the sample.

Figure 3 shows the Scores maps of PC1 (in the 2600–3100 cm^{-1} range) and PC3 (400–800 cm^{-1}) along with histograms displaying the occurrences of Scores values through the different tissues. In both the spectral ranges, there is a clear difference between the BCCO maps on one side and the Ins.+BCCO and Sham maps on the other side. More in detail, the PC3 Score map of the BCCO sample exhibits a brighter color compared to the Ins.+BCCO and Sham maps (Fig. 3a), meaning higher Score values of PC3 as detailed by the corresponding histograms. We have a similar conclusion for the PC1 Score map, where the BCCO map is darker than the others, meaning lower Score values of PC1 (see also the relative histograms). These findings suggest that the calculated PC1 and PC3 components are well-suited spectral parameters to investigate further the effect of BCCO and insulin treatment. Figure 3a and 3b shows a different behavior of BCCO sample compared to Ins.+BCCO and Sham samples. The PC3 histograms (Fig. 3a) show that the PC3 scores distribution of the BCCO sample is centered at larger values than the corresponding distributions of Ins.+BCCO and Sham samples, thus meaning that values of PC3 scores are higher in BCCO sample and lower in Ins.+BCCO and Sham samples.

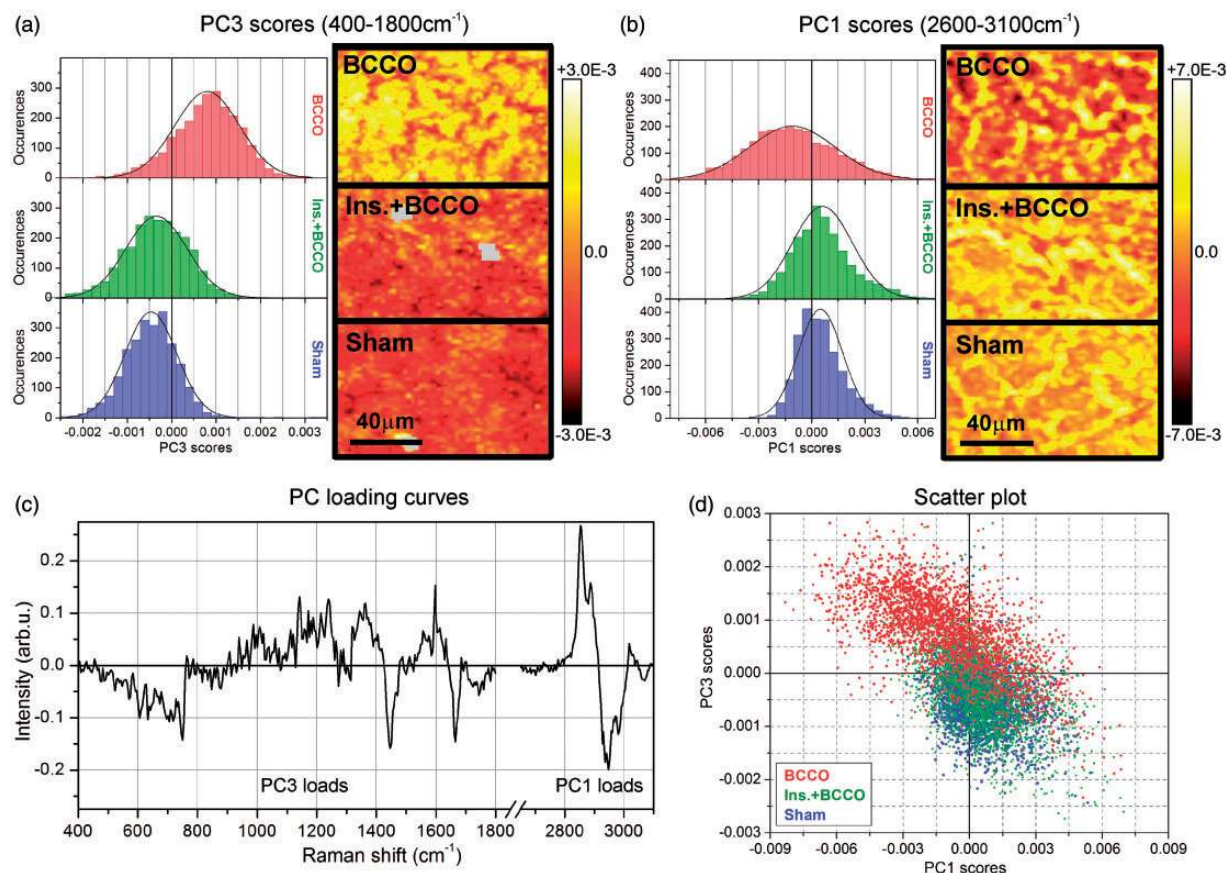


Figure 3. Principal component analysis of Raman maps. Principal component analysis has been performed on the overall data set of Raman spectra recorded for Sham, Ins.+BCCO, and BCCO animals. Subsequently pseudocolor maps are produced by mapping the PC Scores as a function of the x,y coordinates in the 400–1800 cm^{-1} and 2600–3100 cm^{-1} spectral regions. (a) Histograms showing the distribution curves of PC3 scores (400–1800 cm^{-1}) for BCCO, Ins.+BCCO, and Sham samples, along with spatial maps displaying the PC3 scores as color intensities. (b) Histograms of the distribution curves for PC1 scores (2600–3100 cm^{-1}) for the three samples, along with maps displaying the PC1 scores as color intensities. (c) Loading curves of both PC3 (400–800 cm^{-1}) and PC1 (2600–3100 cm^{-1}) which provide an insight in the Raman intensities contributing to PC3 and PC1. (d) Scatter plot of PC3 scores vs. PC1 scores for all the recorded Raman spectra. In both spectral ranges, the BCCO maps and histograms show different behavior in comparison with those of Ins.+BCCO and Sham samples (a, b). This difference is also evident in the scatter plot, where the BCCO spectra (red symbols) significantly deviate from those of Ins.+BCCO and Sham samples (green and blue symbols, respectively).

This same result is also reported as spatial maps of the PC3 scores, displaying the scores values as color intensities in a xy space. Similar differences can be also noticed analyzing the PC1 scores (Fig. 3b): the PC1 histogram of BCCO spectra is centered at smaller values than histograms of Ins.+BCCO and Sham samples, and the corresponding PC1 scores map shows darker colors for the BCCO sample compared to the maps of Ins.+BCCO and Sham samples. The loading curves of PC3 and PC1 are shown in Fig. 3c and provide useful indications on the Raman bands contributing to both PC3 and PC1. The PC1 loading curve, in the 2600–3100 cm^{-1} range, shows one peak at 2850 cm^{-1} and one negative peak (dip) at 2950 cm^{-1} . The literature (see, for example, Freudiger et al.²⁵) widely assumes the former ones as a lipid Raman marker, assigning 2850 cm^{-1}

to CH₂ vibrations, and the latter one as a protein marker, assigning 2950 cm^{-1} to CH₃ vibrations. The PC3 loading curve shows two clear dips at 1445 cm^{-1} (assigned to CH₂) and 1665 cm^{-1} (due to both C=C stretch and Amide I), but also two peaks at 750 cm^{-1} and 1590 cm^{-1} which are characteristic of CytC. The main interest in PC3 loading curve is the shape of these two latter peaks, which exhibit the characteristic profile of a first-derivative of a peak (a so-called “zero-crossing” behavior). Indeed, a closer inspection of both these features shows that they are constituted by a sequence of one dip followed by one peak. At around 750 cm^{-1} , we have a dip at 748 cm^{-1} followed by a peak at 754 cm^{-1} , while at around 1585 cm^{-1} , we have a dip at 1585 cm^{-1} and a peak at 1595 cm^{-1} . This behavior suggests that PC3 is sensitive to variations of

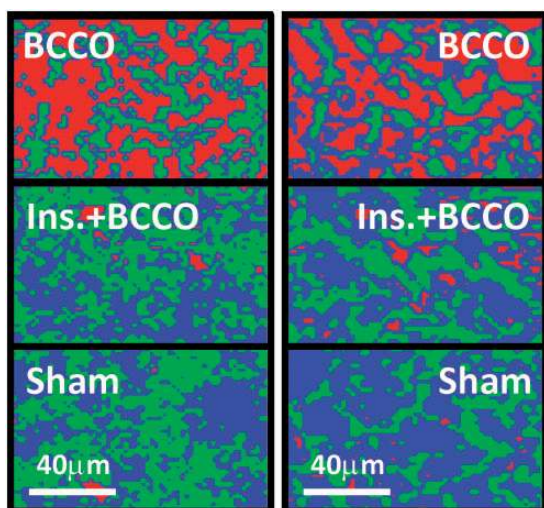


Figure 4. K-means cluster analysis of Raman maps. K-means cluster analysis has been performed on the whole data set of the Raman spectra recorded on the brain tissues of the three groups of animals, separating the two spectral regions $400\text{--}1800\text{ cm}^{-1}$ (left column) and $2600\text{--}3100\text{ cm}^{-1}$ (right column). Clustering procedure has been performed using a number of clusters $K=3$. The ratio of between-group variability to within-group variability (i.e., explained variance/unexplained variance) has been computed for several K -values; the so-called "elbow criterion" indicates that the suitable number of clusters is between $K=3$ and $K=4$. However, the use of $K=4$ clusters only produced a redundant fragmentation of data, without any extra information, and consequently a value $K=3$ has been chosen. K-means cluster analysis shows a clear variation between the BCCO (first row) dominated by the red cluster and the Ins.+BCCO and Sham (second and third rows, respectively) cluster maps where red clusters are nearly absent.

these Raman frequencies for CytC peaks, which across the maps is moving from the dip frequency to the peak frequency.

Subsequently KCA is performed separately on the two spectral regions, $400\text{--}800\text{ cm}^{-1}$ and $2600\text{--}3100\text{ cm}^{-1}$. As a result of KCA, all the spectra are grouped in three clusters labeled with red, green, and blue colors. In both spectral regions, the red cluster is dominantly present in the BCCO sample (Fig. 4). Figure 5 shows the average spectra of each cluster and, despite their similarity, a careful analysis of the major peaks reveals some interesting findings. First, in the $400\text{--}1800\text{ cm}^{-1}$ range, several CytC sharp peaks are clearly visible (located at 750 , 1127 , 1315 , and 1585 cm^{-1}) due to resonant Raman scattering. A meticulous comparison of their spectral position shows that the 1585 cm^{-1} peak undergoes a slight upshift, of about 5 cm^{-1} , of the red cluster curve compared with the green and blue clusters. Even if this shift is only slightly larger than the spectral resolution, the fact that it is occurring mostly in the BCCO sample, and is not equally distributed in the three brain tissues, constitutes a significant result and is not merely a

measurement artifact. Moreover, the other CytC peaks (750 , 1127 , and 1315 cm^{-1}) do not show any shift between the average spectra, thus confirming that the shift observed for the 1585 cm^{-1} peak is a notable one. Instead, in the $2600\text{--}3100\text{ cm}^{-1}$ spectral region, a straightforward comparison of average spectra shows that the red cluster has the lower intensity of the CH_2 vibration (located at 2850 cm^{-1}), which is a typical lipid marker in Raman spectroscopy.

Key Role of Cytochrome C in Raman Detection of Apoptotic Tissue

It has been shown that CytC is not only involved in the respiratory chain but it could be also one of the promoters of cell apoptosis.³⁶ It is now well accepted that early release of CytC from mitochondria into the cytosol leads to the formation of a multi-protein complex, called apoptosome, which in turn activates caspases and consequently apoptosis. The pioneering work of Jemmerson et al.³⁷ remarked that the relevant caspase activator is a membrane-bound CytC and that a conformational change of CytC occurs in dying cells due to their association with intracellular membrane. More recently it has been underlined that CytC is present both tightly and loosely bound to mitochondrial inner membrane, where the loosely bound is responsible for the respiratory activity while the tightly one accounts for peroxidase activity of CytC.^{36,38} More specifically, the oxidation is catalyzed by a cardiolipin-specific peroxidase activity of cardiolipin-bound CytC, which may even occur before the release of proapoptotic factors.³⁹ The interplay between CytC and cardiolipin has been recently studied also by Raman spectroscopy,⁴⁰ evidencing how CytC can induce permeabilization of the mitochondrial membrane which in turn starts the apoptosis process. In these mentioned cases, it is the CytC bound to membrane and/or membrane constituent (i.e., cardiolipin) which plays an important role in cell death and/or cell oxidative damage. In addition, a conformational change of CytC, compared to its native form, is likely to occur due to binding with membrane fatty acids.

In this context, Raman signal from CytC becomes a very sensitive marker for apoptotic processes. Indeed, 532 nm laser radiation is expected to excite resonant Raman scattering of CytC and, consequently, the biochemical Raman features of CytC can be monitored in an augmented way without any additional labeling and/or surface-enhanced Raman scattering (SERS) effect. Former work by Sinibaldi et al.³² has clearly shown that the Raman peak at 1585 cm^{-1} of CytC, assigned to stretching vibration ($\text{C}_\alpha\text{C}_m$)_{asym} (vibration ν_{19} in Hu et al.³⁵), upshifts when binding to oleic acid, due to conformational change, and a similar effect can be reasonably supposed for CytC bound to membrane elements. Consequently, we can assume that the upshift of CytC 1585 cm^{-1} Raman peak observed in

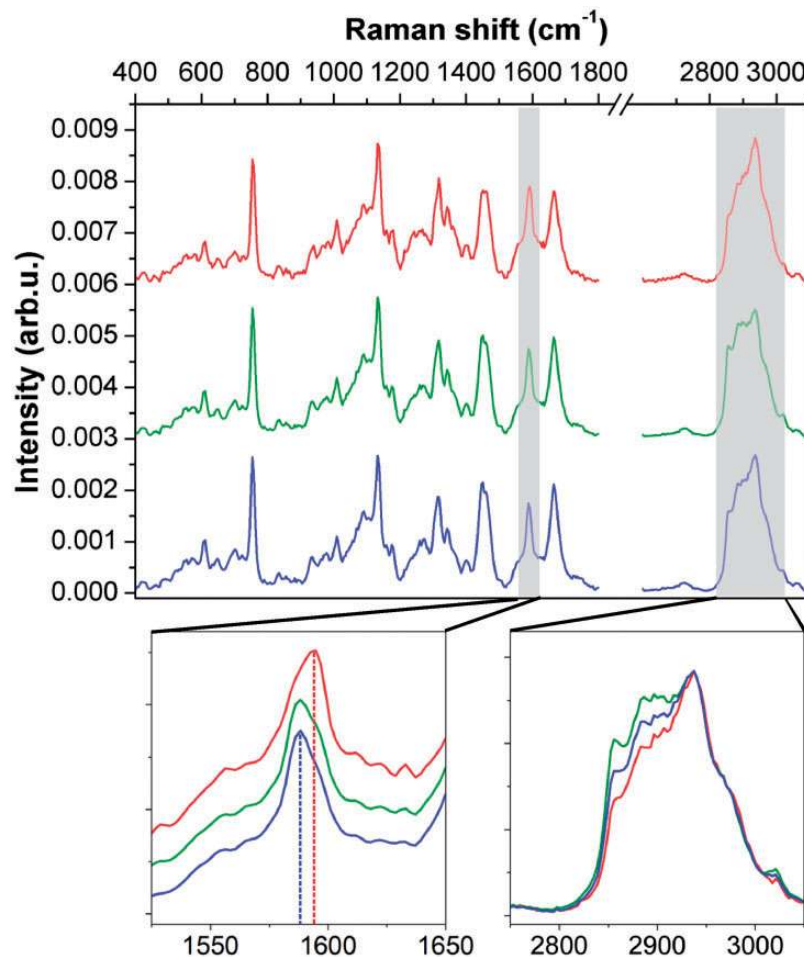


Figure 5. Analysis of the differences between the average spectra from the KCA clusters. The top graph shows the average curves of each cluster coming from KCA analysis: from the top, the first curve corresponds to the red cluster, the second curve to the green cluster, and the third curve to the blue cluster. The three average spectra look very similar each other, but a deeper comparison shows important differences for the 1585 cm^{-1} peak of CytC and for the 2850 cm^{-1} peak of lipids (bottom insets). The 1585 cm^{-1} CytC peak upshifts at higher frequencies for the red cluster, while the 2850 cm^{-1} lipid peak has the smallest intensity for the red cluster. Both these findings indicate a pronounced apoptosis and/or oxidative stress for the red cluster areas.

the BCCO tissue can be ascribed to a large amount of apoptotic and pre-apoptotic cells. In comparison, both the Sham and the Ins.+BCCO tissue do not show this spectral behavior, with Sham and Ins.+BCCO maps (both score and cluster maps) looking very similar each other. These findings support the thesis of an increased apoptotic activity in the CA3 hippocampal region of BCCO animals and show how an accurate analysis of CytC spectral features can provide many details on the health status of tissues and cells.

This conclusion is also supported by the results found in the $2600\text{--}3100\text{ cm}^{-1}$ region. As already mentioned, in the BCCO tissue we can observe a decrease of the lipid peak (2850 cm^{-1}) compared to the protein one (2950 cm^{-1}). Indeed, apoptosis and pre-apoptosis mechanisms are accompanied and even started by oxidative processes.

One major effect of oxidative stress on fatty acids is lipid peroxidation which decreases the intensity of the 2850 cm^{-1} CH_2 peak,^{41,42} as it is observed in the BCCO tissue compared to the Sham and Ins.+BCCO samples.

Conclusion

In this work, histological microscopy and Raman microimaging have demonstrated that insulin treatment prevents apoptotic cell death in the CA3 hippocampal region after BCCO-induced ischemia in MGs. Raman technique has proven to be a straightforward approach (no sample preparation, no labeling) to attain a biochemical framework. The role of CytC in the early stage of cell apoptosis,^{36,37} along with its resonant Raman scattering with 532 nm incident wavelength, has proven that the spectral fingerprint of

CytC is a highly sensitive and significant indicator of the status of the cells. It has been formerly proven⁴⁰ that CytC binding to cardiolipin causes the permeabilization of mitochondrial membrane, then leading to cell apoptosis, and that the high glucose levels reached after ischemic events trigger the CytC release from mitochondria as an apoptotic pathway.⁴³ Activation of IRs helps to prevent the apoptosis induced by high glucose levels; evidence shows that this effect is correlated with the prevention of both CytC release and mitochondrial dysfunction.⁴⁴ However, the mechanism through which the activation of IRs prevents the CytC release is still under investigation.

According to the literature, we suppose that the anti-apoptotic effects observed in the CA3 region may be due to PI-3K signaling, according to evidence demonstrating the role of insulin in blocking CytC release in CA3 neurons after global transient ischemia/reperfusion through activation of PI3-K/Akt pathway⁴⁵ and inhibition of pro-apoptotic factor Bax.^{46–48} Then, the insulin early neuroprotection observed in our experiments is likely due to its ability to counteract oxidative damage of lipids induced by ischemia/reperfusion, preventing CytC detachment from inner mitochondrial membrane.

Acknowledgments

The authors thank Mr. Giovanni Politi for his technical assistance during the animal experiments.

Conflict of Interest

The authors report there are no conflicts of interest.

Funding

This work was supported by Interregional Research Centre for Food Safety & Health (IRC_FSC) (PON a3-00359), by PON03PE_00078_1 and PON03PE_00078_2. Partial support has been also provided by Italian Ministry of Health under the Young Researchers programme financing project GR-2010-2311677 (CUP J65C13001350001) and project GR-2010-2320665 (CUP J65C13001370001).

ORCID iD

Patrizio Candeloro  <https://orcid.org/0000-0001-6156-887X>

References

- M.A. Moskowitz, E.H. Lo, C. Iadecola. "The Science of Stroke: Mechanisms in Search of Treatments". *Neuron*. 2010. 67(2): 181–198.
- J.R. Tan, Y.X. Koo, P. Kaur, et al. "MicroRNAs in Stroke Pathogenesis". *Curr. Mol. Med.* 2011. 11(2): 76–92.
- S.M. Davis, K.R. Lees, G.V. Albers, et al. "Selfotel in Acute Ischemic Stroke: Possible Neurotoxic Effects of An NMDA Antagonist". *Stroke*. 2000. 31(2): 347–354.
- A. Shuaib, K.R. Lees, P. Lyden, et al. "NXY-059 for the Treatment of Acute Ischemic Stroke". *New Engl. J. Med.* 2007. 357(6): 562–571.
- T. Yamaguchi, E. Mori, K. Minematsu, et al. "Alteplase at 0.6 Mg/Kg for Acute Ischemic Stroke within 3 Hours of Onset: Japan Alteplase Clinical Trial (J-ACT)". *Stroke*. 2006. 37(7): 1810–1815.
- Y. Higashi. "Edaravone for the Treatment of Acute Cerebral Infarction: Role of Endothelium-Derived Nitric Oxide and Oxidative Stress". *Expert Opin Pharmacother.* 2009. 10(2): 323–331.
- J. Li, Z. Zeng, B. Viollet, et al. "Neuroprotective Effects of Adenosine Monophosphate-Activated Protein Kinase Inhibition and Gene Deletion in Stroke". *Stroke*. 2007. 38(11): 2992–2999.
- H. Shinichi, F.H. Wakako, T. Shogo. "Ischemic Stroke and Glucose Intolerance: A Review of the Evidence and Exploration of Novel Therapeutic Targets". *J. Pharmacol. Sci.* 2012. 118(1): 1–13.
- R. Ghasemi, A. Haeri, L. Dargahi, et al. "Insulin in the Brain: Sources, Localization and Functions". *Mol. Neurobiol.* 2013. 47(1): 145–171.
- J. Hill, M. Lesniak, C. Pert, et al. "Autoradiographic Localization of Insulin Receptors in Rat Brain: Prominence in Olfactory and Limbic Areas". *Neuroscience*. 1986. 17(4): 1127–1138.
- R.J. Schulz, T.C. Pagano, D. Hung, et al. "Insulin Receptors and Insulin Action in the Brain: Review and Clinical Implications". *Neurosci. Biobehav. Rev.* 2000. 24(8): 855–872.
- J. Mielke, Y. Wang. "Insulin, Synaptic Function, and Opportunities for Neuroprotection". *Prog. Mol. Biol. Transl. Sci.* 2011. 98: 133–186.
- D. Hopkins, G. Williams. "Insulin Receptors are Widely Distributed in Human Brain and Bind Human and Porcine Insulin with Equal Affinity". *Diabet. Med.* 1997. 14(12): 1044–1050.
- C.W. Freudiger, W. Min, B.G. Saar, et al. "Label-Free Biomedical Imaging with High Sensitivity by Stimulated Raman Scattering Microscopy". *Science*. 2008. 322(5909): 1857–1861.
- H. Wu, J.V. Volponi, A.E. Oliver, et al. "In Vivo Lipidomics Using Single-Cell Raman Spectroscopy". *Proc. Natl. Acad. Sci. U. S. A.* 2011. 108(9): 3809–3814.
- M.L. Coluccio, F. Gentile, G. Das, et al. "Detection of Single Amino Acid Mutation in Human Breast Cancer by Disordered Plasmonic Self-Similar Chain". *Sci. Adv.* 2015. 1(8): E1500487.
- F. Zolea, F. Biamonte, P. Candeloro, et al. "H Ferritin Silencing Induces Protein Misfolding in K562 Cells: A Raman Analysis". *Free Radical Biology and Medicine*. 2015. 89: 614–623.
- F. Langenbach, J. Handschel. "Effects of Dexamethasone, Ascorbic Acid and Beta-Glycerophosphate on the Osteogenic Differentiation of Stem Cells in Vitro". *Stem Cell Res. Ther.* 2013. 4(5): 117.
- L. Tirinato, C. Liberale, S. di Franco, et al. "Lipid Droplets: A New Player in Colorectal Cancer Stem Cells Unveiled by Spectroscopic Imaging". *Stem Cells*. 2015. 33(1): 35–44.
- L. Tirinato, F. Gentile, D. Di Mascolo, et al. "SERS Analysis on Exosomes Using Super-Hydrophobic Surfaces". *Microelectronic Engineering*. 2012. 97: 337–340.
- Y. Tan, S.O. Konorov, H.G. Schulze, et al. "Comparative Study Using Raman Microspectroscopy Reveals Spectral Signatures of Human Induced Pluripotent Cells More Closely Resemble those from Human Embryonic Stem Cells than those from Differentiated Cells". *Analyst*. 2012. 137(19): 4509–4515.
- E. Parrotta, M.T. de Angelis, S. Scalise, et al. "Two Sides of the Same Coin? Unraveling Subtle Differences Between Human Embryonic and Induced Pluripotent Stem Cells by Raman Spectroscopy". *Stem Cell Research and Therapy*. 2017. 8: 271.
- R. Wolthuis, M. Van Aken, K. Fountas, et al. "Determination of Water Concentration in Brain Tissue by Raman Spectroscopy". *Anal. Chem.* 2001. 73(16): 3915–3920.
- L.-L. Tay, R.G. Tremblay, J. Hulse, et al. "Detection of Acute Brain Injury by Raman Spectral Signature". *Analyst*. 2011. 136(8): 1620–1626.
- C.W. Freudiger, R. Pfannl, D.A. Orringer, et al. "Multicolored Stain-Free Histopathology with Coherent Raman Imaging". *Lab. Invest.* 2012. 92: 1492–1502.
- A. Dutta, R. Gautam, S. Chatterjee, et al. "Ascorbate Protects Neurons Against Oxidative Stress: A Raman Microspectroscopic Study". *ACS Chem. Neurosci.* 2015. 6(11): 1794–1801.
- G.B. Jung, S.W. Kang, G.-L. Lee, et al. "Biochemical Characterization of the Brain Hippocampal Areas After Cerebral Ischemia-Reperfusion

- Using Raman Spectroscopy". *Appl. Spectrosc.* 2018. 72(10): 1479–1486.
28. J.R. Ferraro, K. Nakamoto. *Introductory Raman Spectroscopy*. Amsterdam: Academic Press, 2003.
 29. C. Matthaus, T. Chernenko, L. Quintero, et al. "Raman Micro-Spectral Imaging of Cells and Intracellular Drug Delivery Using Nanocarrier Systems". In: T. Dieing, O. Hollricher, J. Toporski, editors. *Confocal Raman Microscopy*. Berlin; Heidelberg: Springer-Verlag, 2010. Pp: 137–163.
 30. T. Rajalahti, O.M. Kvalheim. "Multivariate Data Analysis in Pharmaceutics: A Tutorial Review". *Int. J. Pharm.* 2011. 417(1–2): 280–290.
 31. P. Candeloro, E. Grande, R. Raimondo, et al. "Raman Database of Amino Acids Solutions: A Critical Study of Extended Multiplicative Signal Correction". *Analyst*. 2013. 138(24): 7331–7340.
 32. F. Sinibaldi, G. Mei, F. Polticelli, et al. "ATP Specifically Drives Refolding of Non-Native Conformations of Cytochrome C". *Protein Sci.* 2005. 14: 1049–1058.
 33. C. Krafft, T. Knetschke, R.H.W. Funk, et al. "Identification of Organelles and Vesicles in Single Cells by Raman Microspectroscopic Mapping". *Vib. Spectrosc.* 2005. 38(1–2): 85–93.
 34. D.S. Read, D.J. Woodcock, N.J. Strachan, et al. "Evidence for Phenotypic Plasticity Among Multihost *Campylobacter jejuni* and *C. coli* Lineages, Obtained Using Ribosomal Multilocus Sequence Typing and Raman Spectroscopy". *Appl. Env. Microbiol.* 2013. 79(3): 965–973.
 35. S. Hu, I.K. Morris, J.P. Singh, et al. "Complete Assignment of Cytochrome C Resonance Raman Spectra Via Enzymic Reconstitution with Isotopically Labeled Hemes". *J. Am. Chem. Soc.* 1993. 115(26): 12446–12458.
 36. C. Garrido, L. Galluzzi, M. Brunet, et al. "Mechanisms of Cytochrome C Release from Mitochondria". *Cell Death Differ.* 2006. 13: 1423–1433.
 37. R. Jemmerson, J. Liu, D. Hausauer, et al. "A Conformational Change in Cytochrome C of Apoptotic and Necrotic Cells Is Detected by Monoclonal Antibody Binding and Mimicked by Association of the Native Antigen with Synthetic Phospholipid Vesicles". *Biochem.* 1999. 38(12): 3599–3609.
 38. V.E. Kagan, G.G. Borisenko, Y.Y. Tyurina, et al. "Oxidative Lipidomics of Apoptosis: Redox Catalytic Interactions of Cytochrome C with Cardiolipin and Phosphatidylserine". *Free Radic. Biol. Med.* 2004. 37(12): 1963–1985.
 39. V.E. Kagan, V.A. Tyurin, J. Jiang, et al. "Cytochrome C Acts as a Cardiolipin Oxygenase Required for Release of Proapoptotic Factors". *Nat. Chem. Biol.* 2005. 1: 223–232.
 40. J.P. Kitt, D.A. Bryce, S.D. Minter, et al. "Raman Spectroscopy Reveals Selective Interactions of Cytochrome C with Cardiolipin that Correlate with Membrane Permeability". *J. Am. Chem. Soc.* 2017. 139(10): 3851–3860.
 41. N.S. Ozek, S. Tuna, A.E. Erson-Bensan, et al. "Characterization of MicroRNA-125b Expression in MCF7 Breast Cancer Cells by ATR-FTIR Spectroscopy". *Analyst*. 2010. 135(12): 3094–3102.
 42. M.D. Guillen, N. Cabo. "Some of the Most Significant Changes in the Fourier Transform Infrared Spectra of Edible Oils Under Oxidative Conditions". *J. Sci. Food. Agric.* 2000. 80: 2028–2036.
 43. D.A. Allen, M.M. Yaqoob, S.M. Harwood. "Mechanisms of High Glucose-Induced Apoptosis and Its Relationship to Diabetic Complications". *J. Nutr. Biochem.* 2005. 16(12): 705–713.
 44. Y. Li, H. Wu, R. Khardori, et al. "Insulin-Like Growth Factor⁻¹ Receptor Activation Prevents High Glucose-Induced Mitochondrial Dysfunction, Cytochrome-C Release and Apoptosis". *Biochem. Biophys. Res. Commun.* 2009. 384(2): 259–264.
 45. P.R. Shepherd, D.J. Withers, K. Siddle. "Phosphoinositide 3-Kinase: The Key Switch Mechanism in Insulin Signaling". *Biochem. J.* 1998. 333: 471–490.
 46. S.J. Gardai, D.A. Hildeman, S.K. Frankel, et al. "Phosphorylation of Bax Ser184 by Akt Regulates its Activity and Apoptosis in Neutrophils". *J. Biol. Chem.* 2004. 279(20): 21085–21095.
 47. T.H. Sanderson, R. Kumar, J.M. Sullivan, et al. "Insulin Blocks Cytochrome C Release in the Reperfused Brain Through PI3-K Signaling and by Promoting Bax/Bcl-XL Binding". *J. Neurochem.* 2008. 106(3): 1248–1258.
 48. T.H. Sanderson, R. Kumar, A.C. Murariu-Dobrin, et al. "Insulin Activates the PI3K-Akt Survival Pathway in Vulnerable Neurons Following Global Brain Ischemia". *Neuro. Res.* 2009. 31(9): 947–958.